Molecular Cell, Vol. 18, 589–599, May 27, 2005, Copyright ©2005 by Elsevier Inc. DOI 10.1016/j.molcel.2005.04.016

The 1.9 Å Structure of a Proteasome-11S Activator Complex and Implications for Proteasome-PAN/PA700 Interactions

Andreas Förster,[1] Eugene I. Masters,[1] Frank G. Whitby,[1] Howard Robinson,[2] and Christopher P. Hill[1,*]
[1]Department of Biochemistry
University of Utah School of Medicine
Salt Lake City, Utah 84132
[2]Biology Department
Brookhaven National Laboratory
Upton, New York 11973

Summary

Proteasomes are cylindrical structures that function in multiple cellular processes by degrading a wide variety of cytosolic and nuclear proteins. Substrate access and product release from the enclosed catalytic chamber occurs through axial pores that are opened by activator complexes. Here, we report high-resolution structures of wild-type and mutant archaeal proteasomes bound to the activator PA26. These structures support the proposal that an ordered open conformation is required for proteolysis and that its formation can be triggered by outward displacement of surrounding residues. The structures and associated biochemical assays reveal the mechanism of binding, which involves an interaction between the PA26 C terminus and a conserved lysine. Surprisingly, biochemical observations implicate an equivalent interaction for the unrelated ATP-dependent activators PAN and PA700.

Introduction

Proteasomes (a.k.a., 20S proteasomes or "core particles") are proteases that are responsible for regulated degradation of a large variety of target proteins in the cytosol and nucleus of eukaryotes. The importance of this activity is demonstrated by the observation that proteasome subunits are essential in yeast (Heinemeyer et al., 1994; Velichutina et al., 2004). Proteasomes are comprised of a cylindrical arrangement of four stacked rings, with the two outer rings each containing seven α subunits and the two central rings each containing seven β subunits. Seven different α subunits (α1–α7) and seven different β subunits (β1–β7) occupy unique positions within their respective rings (Eleuteri et al., 1997; Groll et al., 1997; Hilt et al., 1993; Kopp et al., 1997). Proteasomes are also found in some archaea and bacteria, where they usually have a simpler subunit arrangement. For example, the proteasome from the archaeon *Thermoplasma acidophilum* has just one type of α and one type of β subunit, each of which are assembled into homomeric 7-fold symmetric rings.

Proteasomes avoid indiscriminate proteolysis by virtue of their architecture, which sequesters their proteolytic sites in the central chamber of their hollow structure (Groll et al., 1997; Löwe et al., 1995; Unno et al., 2002). Substrates enter the proteasome by passing through an axial pore in the center of the α rings in a process that is facilitated by activating complexes that bind to one or both rings of α subunits. In the *T. acidophilum* proteasome structure, the first 12 residues of the α subunits are disordered, leaving a path into the proteasome interior that is accessible to peptide substrates (Löwe et al., 1995). In contrast, in isolated eukaryotic proteasomes, the N termini of the α subunits are ordered and form a closed conformation, which explains why purified eukaryotic proteasomes show only weak activity against small peptide substrates in vitro (Groll et al., 1997).

Three different kinds of proteasome activator have been identified. PA700 (also called 19S or "regulatory complex") is an ATP-dependent activator that together with the proteasome forms the eukaryotic 26S proteasome that mediates degradation of ubiquitylated proteins (Bochtler et al., 1999). PA700 is a large complex composed of six ATPase subunits and at least 11 other proteins that recognizes, unfolds, and translocates substrate into the proteasome interior. Its archaeal (*M. jannaschii*) analog, PAN, is a homooligomer of ATPase subunits that also mediates protein unfolding and facilitates degradation by proteasome (Benaroudj and Goldberg, 2000; Zwickl et al., 1999). In contrast, the heptameric 11S activators (also called PA28 or REG in most organisms and PA26 in *Trypanosoma brucei*) are ATP independent and stimulate the degradation of peptides but not proteins (Dubiel et al., 1992; Ma et al., 1992). The crystal structure of the human 11S activator PA28α/REGα revealed a toroidal complex with an axial pore large enough to allow transit of peptides (Knowlton et al., 1997). The biological role for 11S activators is not entirely clear. Some homologs apparently function in the production of ligands for presentation by MHC class I complexes, although the mechanistic basis for this role is unknown and some 11S activators must perform other functions (Rechsteiner and Hill, 2005). A third kind of activator, PA200, was recently reported (Ustrell et al., 2002).

Important elements of proteasome activation by 11S activators were revealed by the 3.2 Å resolution crystal structure of yeast (*S. cerevisiae*) proteasome in complex with PA26 (Förster et al., 2003; Whitby et al., 2000). Key findings were that the activator C termini, which provide binding energy (Li et al., 2000; Ma et al., 1993; Song et al., 1997), insert into pockets between the proteasome α subunits (although details were not clear in the low-resolution structure), and that repositioning of a reverse turn on the proteasome surface induces gate opening by destabilizing the closed conformation and allowing four conserved proteasome residues to form a stable cluster.

Opening of the proteasome gate explains much, perhaps all, of the mechanism of stimulation by 11S activators. The possibility that other activators function, at least in part, by stabilizing the same open conformation was suggested by the finding that the conserved cluster residues are also important for PAN-mediated prote-

*Correspondence: chris@biochem.utah.edu

olysis by *T. acidophilum* proteasome (Förster et al., 2003). Important outstanding questions include: what are the specific interactions of the 11S C termini, what are the structural consequences of inactivating proteasome mutations, how are archaeal proteasomes, which generally have disordered closed gate conformations, induced to assume a fully open conformation, and to what extent are mechanisms of binding and activation shared by the different unrelated activators?

In an effort to understand the mechanism of proteasome activation further, we have determined the 2.3 Å structure of *T. acidophilum* proteasome in complex with PA26, which reveals the same open gate conformation as seen earlier in the low-resolution yeast proteasome-PA26 complex and implies that formation of the open conformation requires outward displacement of a set of reverse turns surrounding the gate. We also report 1.9 Å and 2.4 Å structures of PA26 complexes with two *T. acidophilum* proteasome mutants, which supports the model that formation of an ordered open gate conformation is necessary for proteolysis. These high-resolution structures show how the highly variable 11S C-terminal residues bind proteasome. Remarkably, this interaction is analogous to that of HslUV, a relatively simple bacterial analog of the 26S proteasome, suggesting that such interactions might be a conserved feature of activator-proteasome complexes. We therefore performed biochemical studies with *T. acidophilum* proteasome and PAN, supporting the proposal of an equivalent interaction for this activator and, by inference, also for the eukaryotic PA700 activator.

Results and Discussion

Structure Determination

11S activators stimulate proteasomes from a wide variety of species. For example, PA26 activates rat (Yao et al., 1999) and yeast (Whitby et al., 2000) proteasomes, human PA28α activates cow (E.I.M., unpublished data) and yeast (M. Rechsteiner, personal communication) proteasomes, and cow PA28 activates lobster proteasome (Mykles, 1996). This promiscuity justified our earlier determination of the 3.2 Å crystal structure of the noncognate yeast proteasome-*T. brucei* PA26 complex (Whitby et al., 2000) and motivated further effort to develop a simpler model system that might provide improved resolution. We chose to work with the archaeal *T. acidophilum* proteasome because it can be produced recombinantly in *E. coli* and is amenable to biochemical analysis of mutant proteins. Because unliganded archaeal proteasomes generally have a disordered gate that is permeable to small model substrates, simple activity assays are not an effective approach to revealing interactions with 11S activators. Instead, we used sedimentation velocity analysis to demonstrate a direct interaction between PA26 and *T. acidophilum* proteasome in solution. PA26 was then crystallized in complex with three different proteasome variants, wild-type (wt) and two mutants, Tyr8Gly/Asp9Gly (GG) and Asp9Ser (D9S), that are inactive in PAN-dependent proteolysis assays (Förster et al., 2003).

All three complexes crystallized under similar conditions, and crystals were essentially isomorphous. In each case, a crystallographic 2-fold axis passes through the center of the complex to leave one PA26 heptamer and one half proteasome in the asymmetric unit. The structure determination was performed by molecular replacement using the known structure of unbound *T. acidophilum* proteasome (Löwe et al., 1995), and PA26 from the yeast proteasome complex (Förster et al., 2003) was docked into the resultant difference density. The high resolution of these structures (wt, 2.3 Å; GG, 2.4 Å; D9S, 1.9 Å) has allowed for effective refinements and revealed previously obscure details of the protein structures and interactions. The R factors for wt, GG, and D9S are 18.0%, 18.0%, and 18.2%, respectively, and the free R values are 22.4%, 23.3%, and 21.6%, respectively. See the Supplemental Data, available with this article online, for crystallographic statistics.

Comparison of Proteasome Structures

All three *T. acidophilum* proteasome-PA26 complex structures are essentially identical (Figure 1A) except in the proteasome pore region (below). The pairwise rmsd over 4300 equivalent Cα atoms of the entire half complexes is ~0.3 Å. The proteasome structures seen here in complex with PA26 also closely resemble the structures of unbound *T. acidophilum* proteasome (Löwe et al., 1995) (rmsd of 0.8 Å over 2930 Cα atoms) and the proteasome from *Archaeoglobus fulgidus* (Groll et al., 2003) (rmsd of 1.2 Å over 2667 Cα atoms). The conformations of three surface loops in proteasome α subunits (residues 59–65, 51–56, and 202–205) vary from the positions seen in the uncomplexed archaeal proteasomes, although these apparent differences are unlikely to be significant because these residues are distant from the PA26 binding surface and have high temperature factors.

The remarkable cross-species activity of 11S activators is explained by comparison of structures and sequences. An alignment of yeast, human, and *T. acidophilum* proteasome sequences shows identity of almost 70% for all 126 (7 × 18) residues that contact PA26 in the yeast and archaeal complexes (Figure 1). These residues are also highly conserved in other species (data not shown). Furthermore, these residues exhibit a high degree of structural similarity. For example, in the closed conformations of isolated yeast (Groll et al., 1997) and bovine proteasomes (Unno et al., 2002), the 126 α ring interface residues superimpose with an rmsd of 0.7 Å on Cα atoms. More significantly, in the open conformations of yeast and *T. acidophilum* proteasomes in complex with PA26, the same interface residues superimpose with an rmsd of 1.2 Å on Cα atoms. Therefore, the reason 11S activators are able to activate proteasomes from a wide variety of species is that the interaction surface of all proteasomes is highly conserved in both sequence and structure.

The Internal Loop of PA26

Model building of PA26 in the original yeast proteasome complex was challenging due to the limited resolution, high overall B factor, and the lack of a high-resolution structure of unliganded PA26 (Förster et al., 2003; Whitby et al., 2000). Comparison with the high-resolu-

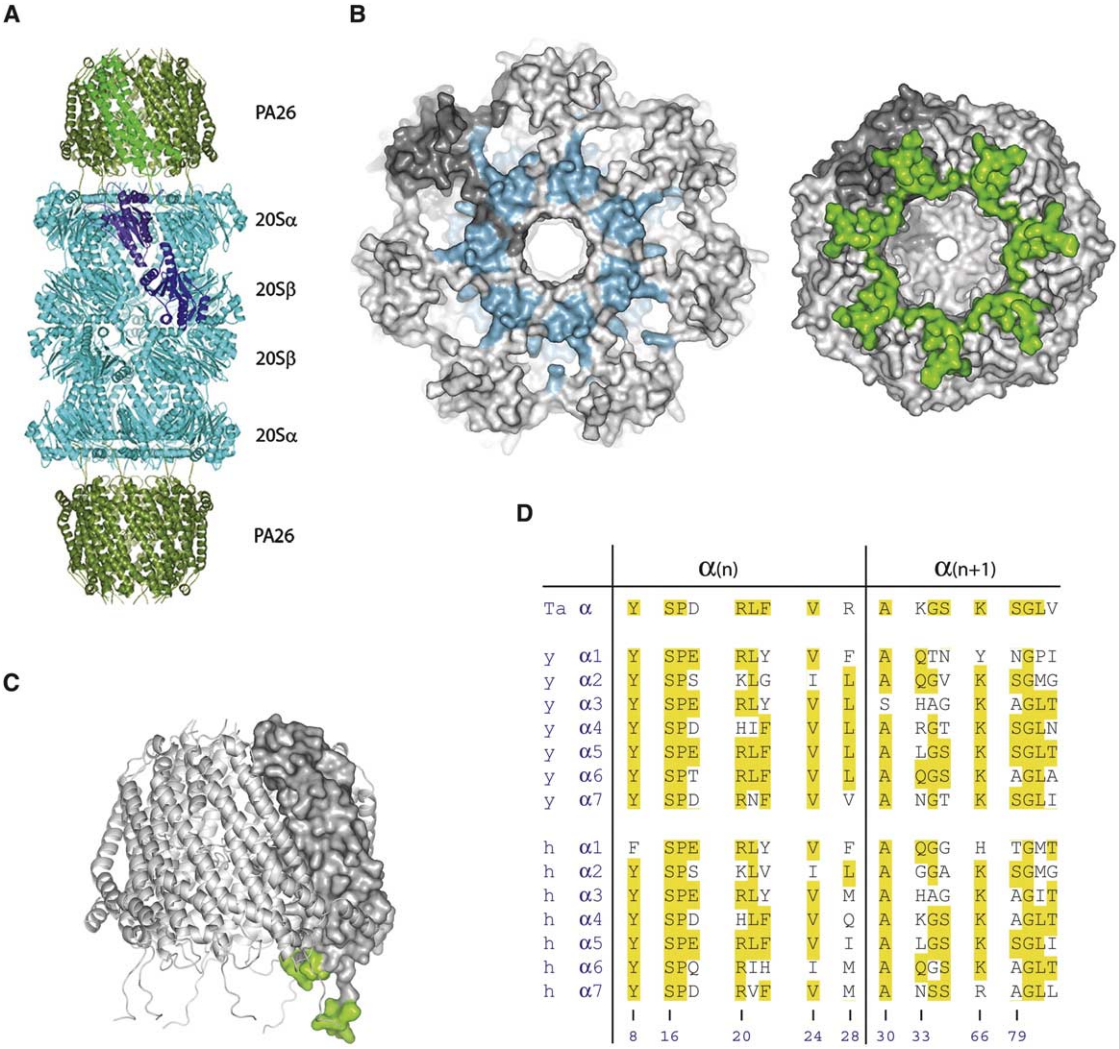

		α(n)					α(n+1)			
Ta	α	Y	SPD	RLF	V	R	A	KGS	K	SGLV
y	α1	Y	SPE	RLY	V	F	A	QTN	Y	NGPI
y	α2	Y	SPS	KLG	I	L	A	QGV	K	SGMG
y	α3	Y	SPE	RLY	V	L	S	HAG	K	AGLT
y	α4	Y	SPD	HIF	V	L	A	RGT	K	SGLN
y	α5	Y	SPE	RLF	V	L	A	LGS	K	SGLT
y	α6	Y	SPT	RLF	V	L	A	QGS	K	AGLA
y	α7	Y	SPD	RNF	V	V	A	NGT	K	SGLI
h	α1	F	SPE	RLY	V	F	A	QGG	H	TGMT
h	α2	Y	SPS	KLV	I	L	A	GGA	K	SGMG
h	α3	Y	SPE	RLY	V	M	A	HAG	K	AGIT
h	α4	Y	SPD	HLF	V	Q	A	KGS	K	AGLT
h	α5	Y	SPE	RLF	V	I	A	LGS	K	SGLI
h	α6	Y	SPQ	RIH	I	M	A	QGS	K	AGLT
h	α7	Y	SPD	RVF	V	M	A	NSS	R	AGLL
		8	16	20	24	28	30	33	66	79

Figure 1. Structure of *Thermoplasma acidophilum* Proteasome-PA26

(A) Crystal structure of *T. acidophilum* proteasome-PA26 viewed along a molecular 2-fold axis. Seven-fold axis is vertical. Individual PA26 and proteasome α and β subunits are highlighted in one half of the complex.

(B) Contact surfaces. Left: proteasome. Right: PA26. Contact residues (atom within 4.0 Å) are colored. One subunit is shaded darker gray.

(C) PA26 side view. One subunit is shown as a surface representation, the other six as semitransparent cartoons. In the surface representation, residues that contact the proteasome (i.e., activation loop and C-terminal tails) are colored green.

(D) Proteasome residues within 4.0 Å of PA26. Sequences for *T. acidophilum*, Ta; *Saccharomyces cerevisiae,* y; and human, h. The most conserved residue for each position is shown on a yellow background. Numbering throughout the manuscript is for the *T. acidophilum* proteasome sequence. Each PA26 subunit contacts residues from two adjacent (n and n + 1) α subunits, as indicated.

tion structures now obtained in complex with *T. acidophilum* proteasome reveals that the earlier model of PA26 is mostly correct, although two important features are only now resolved. First, the C-terminal residues, which were barely visible in the yeast complex, are now clearly defined and reveal important details of proteasome binding (below). Second, helix 3 is now seen to be interrupted by an unusual 14-residue insertion that projects into the central channel of the PA26 heptamer (Figure 2). Building of this loop causes a corresponding frameshift in the C-terminal half of helix 3 and shortens the disordered loop between helices 3 and 4 to 12 residues. In the heptamer, the seven internal loops form a diaphragm-like structure that, in the absence of conformational change, would prevent passage of small molecules such as the fluorogenic peptide substrates used in standard activity assays (Figures 1B and 2).

Reexamination of omit maps for the yeast proteasome-PA26 structure confirmed that PA26 possesses the internal loop in this complex as well, although details of its conformation are different in the yeast and *T. acidophilum* proteasome complexes. In particular, whereas the loop is well ordered in the *T. acidophilum* proteasome complexes it is largely disordered in the yeast proteasome complex, where density is very clear for helix 3 (except for a gap at the position of the insertion) but essentially absent for most of the loop. One possibility is that this loop is ordered at the low pH

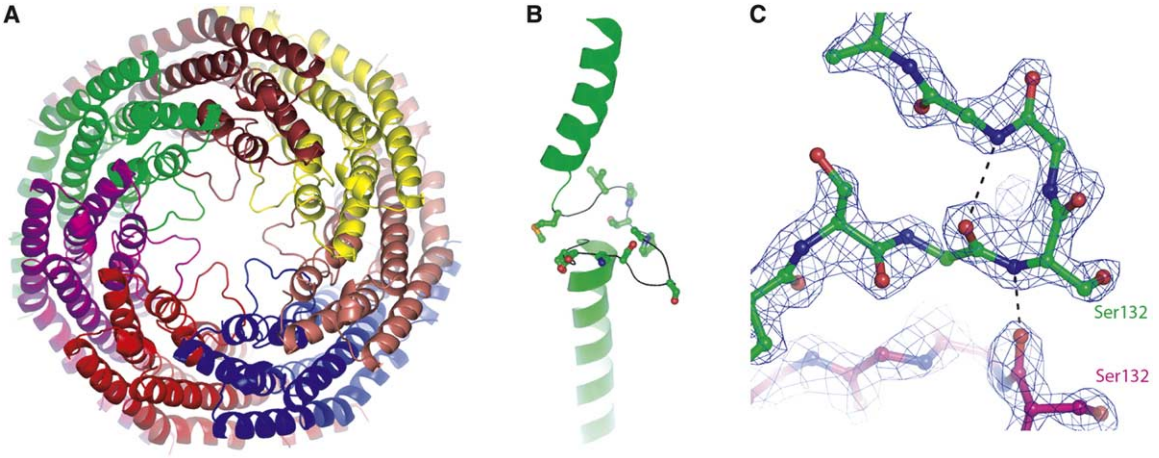

Figure 2. The Internal Loop of PA26

(A) PA26 viewed along the 7-fold axis from the direction of the proteasome. The internal loop forms a diaphragm-like structure.

(B) Side view of helix 3 with the internal loop. The green subunit in panel (A) has been rotated by 90° about the horizontal axis.

(C) Omit density map for the loop region. For map calculation, the occupancy of PA26 residues 120–150 was set to zero, all atoms in the model were randomly shifted by an average of 0.5 Å, and maps were created after five cycles of restrained refinement in REFMAC5 (Murshudov, 1997). Contour level is 1.5 × rmsd. Orientation is similar to that of panel (A).

(5.6) of crystallization with *T. acidophilum* proteasome but is mobile at the neutral pH (7.5) of the yeast *T. acidophilum* complex crystals. It is notable that in the *T. acidophilum* proteasome complexes a hydrogen bond apparently exists between carboxylate oxygens of Glu129 in the loop and Glu147 in helix 3 of the adjacent subunit. At the higher pH of yeast proteasome-PA26 crystals, however, this interaction is not expected to form because both glutamates will be deprotonated. Consistent with this view, regions of the internal loop whose conformation is defined in the yeast proteasome complex shows that the separation between Glu129 and Glu147 is too great to accommodate hydrogen bond formation.

The internal loop sequence (SGEKSGSGGAPTPI) possesses a predominance of small side chains. Two of the four glycines may be required to adopt the observed conformation because Gly135 has torsion angles that are disallowed for other residues and Gly128 appears unable to accommodate a Cβ atom without some structural rearrangement. However, the other two glycine residues do not appear to be required for this structure. We therefore suggest that the large number of small residues in the loop might further increase flexibility at neutral pH. In the *T. acidophilum* D9S proteasome-PA26 structure, the main chain atoms of the internal loop are well defined (temperature factors between 30 and 40 $Å^2$), but for wild-type and GG proteasomes, the potential for flexibility is revealed by temperature factors between 50–75 $Å^2$ and 60–85 $Å^2$, respectively, which is significantly higher than the average for PA26 in these structures. We therefore suggest that this loop is highly flexible in vivo and allows passage of peptide substrate/products in/out of the proteasome.

Comparison of PA26 and PA28

PA26 is highly diverged from the other 11S activators, all of which are called PA28 and share 35%–50% sequence identity with each other in pairwise comparisons. Initial inspection of sequences suggested that the closest relative of PA26 is the α isoform of PA28 (Yao et al., 1999). Comparison of the human PA28α crystal structure (Knowlton et al., 1997) with PA26 from the *T. acidophilum* proteasome complex now reveals a pairwise alignment in which 931 Cα atoms (133 per subunit) overlap with an rmsd of 1.7 Å (Figure 3A). These structurally conserved residues are located in helices 2, 3, and 4; 31 of them (23%) have the same amino acid identity in PA26 and hPA28α, and 12 (9%) are invariant in all three human 11S activator isoforms. This corresponds to just 5.2% structural and sequence identity over all 231 PA26 residues. The major structural differences between PA26 and PA28α, and presumably other PA28 homologs, are helix 3, which is continuous in PA28α and does not have an internal loop projecting into the central channel, and the lengths of the loops connecting helices 1 and 2 and helices 3 and 4, both of which are distant from the proteasome binding surface.

There is also a significant difference in conformation between the PA26 and PA28α activation loops, with equivalent Cα atoms diverging by up to 3.7 Å after global overlap. This is surprising because in PA26 these residues contact the proteasome to induce gate opening (Förster et al., 2003; Whitby et al., 2000). Specifically, gate opening appears to result from interactions between the PA26 Glu102 side chain and proteasome residues flanking αPro17. Alignment based upon Cα coordinates suggests that PA26 Glu102 is equivalent to PA28α Gly145, a residue that is unable to mediate equivalent interactions with proteasome. Due to the different paths of PA26 and PA28α activation loops, however, the side chain of the adjacent PA28α residue, Asp144, overlaps the position of the PA26 Glu102 side chain (Figure 3B). Because PA28α Asp144 is conserved in all PA28 isoforms, we propose that it mediates activating interactions analogous to those seen for PA26

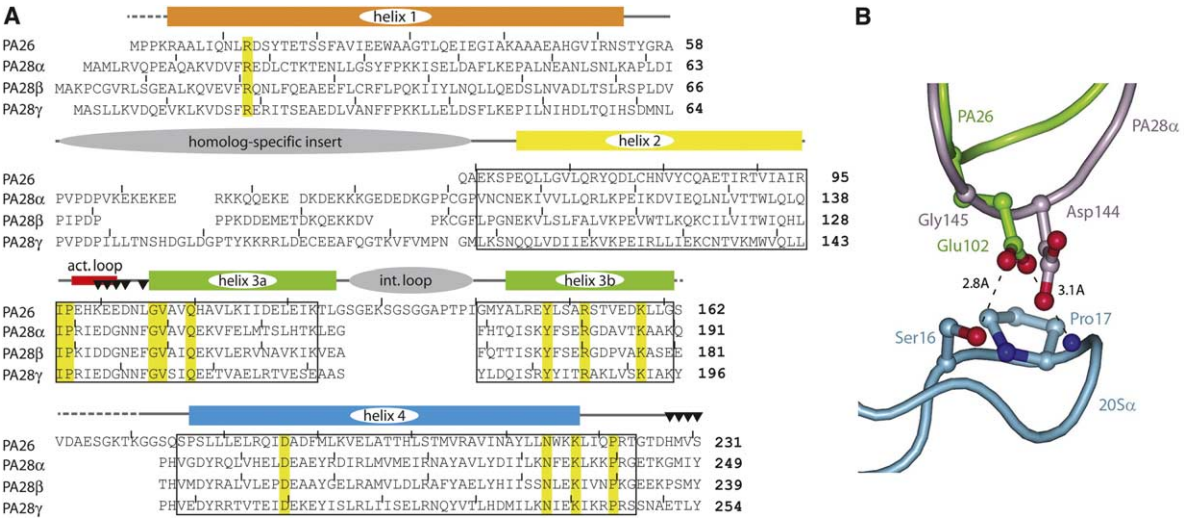

Figure 3. Comparison of PA26 and PA28

(A) Structure-based sequence alignment of PA26 and the three human PA28 homologs. PA26 secondary structure, above. Disordered residues in PA26 are indicated with a dotted line. Residues with the same identity in all four proteins are shown on a yellow background. Residues that appeared structurally equivalent upon visual inspection of an overall alignment are boxed and were used to obtain the optimal global alignment of PA26 and PA28α. The red bar denotes the activation loop (Zhang et al., 1998). Black triangles denote residues that are within 4.0 Å of the proteasome.

(B) PA26 Glu102 and PA28α Asp144 may make equivalent interactions with the proteasome αPro17 reverse turn. Activation loops are shown after overlap of PA26 and PA28α on residues boxed in panel (A). Cα atoms of PA26 Glu102 and PA28α Gly145 are 2.3 Å apart. PA26 Glu102 and PA28α Asp144 Cα atoms are 3.6 Å apart, but their carboxyl carbons are separated by only 1.6 Å when Asp144 is repositioned as a preferred rotamer. Minor adjustments would allow PA28α Asp144 to adopt equivalent hydrogen bonds as PA26 Glu102.

Glu102. Thus, although the activation loops of PA26 and PA28 differ, both classes of 11S activator might place a side chain carboxylate in similar positions where it can induce gate opening by hydrogen bonding with the αPro17 reverse turn.

Mechanism of Pore Opening

The yeast proteasome-PA26 structure showed that gate opening results, in part, from interactions of the PA26 activation loop that reposition the αPro17 reverse turns and thereby displace more N-terminal residues and destabilize the multiple hydrogen bond and van der Waals interactions of α2, α3, and α4 that define the closed conformation (Whitby et al., 2000). Although necessary, destabilization of the closed conformation is not sufficient for formation of the open conformation because destabilization of the closed gate by mutagenesis causes disordering of the yeast proteasome pore but does not induce the ordered open state (Groll et al., 2000). The yeast proteasome-PA26 structure indicated that the open conformation is stabilized by interactions within a cluster of four conserved proteasome residues (αTyr8, αAsp9, αPro17, and αTyr26 from each subunit). Although these residues make only peripheral contact with PA26 (Figure 1D), mutagenesis studies confirmed that they are important for PAN-mediated proteolysis (Förster et al., 2003). The importance of this conserved cluster is now further supported by the high-resolution wild-type *T. acidophilum* proteasome-PA26 structure reported here, which, compared to the yeast proteasome-PA26 structure, shows an rmsd of just 1.3 Å for overlap of all atoms of the ring of conserved cluster residues (Figure 4).

The importance of the cluster residues is reinforced by the crystal structures of the two mutant *T. acidophilum* proteasome complexes. In both cases, these structures are very similar to the wild-type complexes except that proteasome α subunit residues N-terminal to Thr13 are disordered. The GG mutant removes 14 side chains from the proteasome pore and its disordered gate conformation confirms that this variant has increased mobility in the pore region. This supports the hypothesis that flexibility, while adequate for passage of model peptide substrates, is not sufficient for efficient degradation of protein substrates (Benaroudj et al., 2003; Förster et al., 2003). The D9S mutant occurs naturally in one of the seven α subunits of eukaryotic proteasomes but, like GG, has a debilitating effect on PAN-dependent protease activity when present in all seven subunits of the archaeal proteasome (Förster et al., 2003). The disordered gate structure observed in the D9S-PA26 crystal structure supports the hypothesis that, although this substitution is required in the α2 subunit to form the precisely ordered closed conformation of unbound eukaryotic proteasomes, it is unable to adopt the open conformation and thereby support proteolysis when present in all seven subunits of an α ring.

Upon binding of PA26, the yeast proteasome α subunits pivot outward about their main point of contact with β subunits (102–104 loop). This rigid body rotation is largest for subunits α3 and α4, where it reaches about 5°. The αPro17 reverse turns also move upon

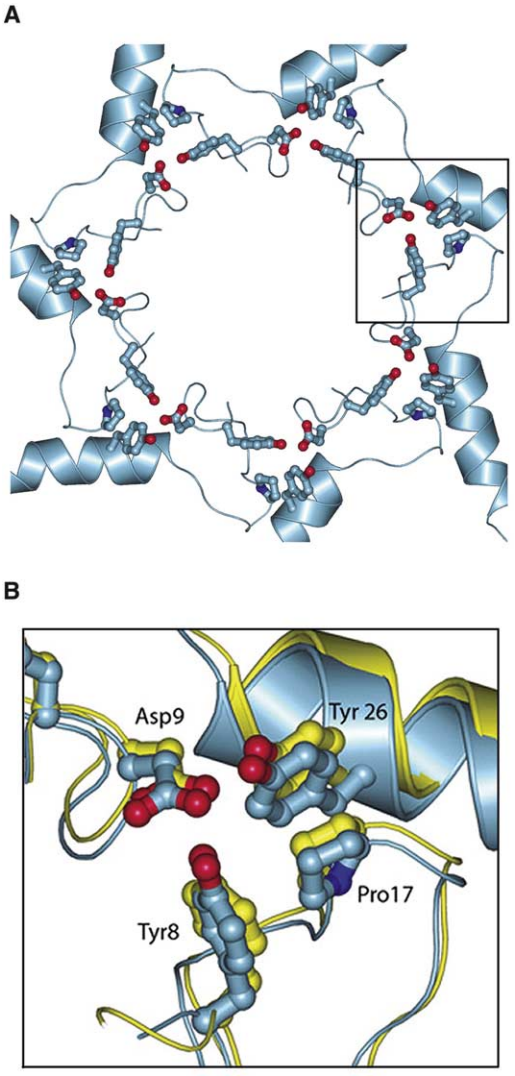

Figure 4. Pore Conformation

(A) The clusters of conserved residues (αTyr8, αAsp9, αPro17, and αTyr26) that stabilize the open conformation are shown.

(B) Enlarged view of cluster boxed in panel (A). *T. acidophilum* proteasome, blue; yeast proteasome, yellow. Both proteasome structures shown as seen in complex with PA26 after global alignment of the rings of α subunits.

binding of PA26, with the average αPro17 Cα displacement being 2.2 Å. In contrast, *T. acidophilum* α subunits do not undergo significant rotation upon binding PA26 nor do the αPro17 reverse turns move by more than 1.0 Å. This raises the question of how binding of PA26 induces *T. acidophilum* proteasome to adopt the ordered open conformation, and the answer is provided by close inspection of the structures. Although the bound and unbound *T. acidophilum* proteasome structures are very similar, there is a small but apparently significant radial displacement of all seven αPro17 reverse turns by almost 1.0 Å upon binding of PA26. This shift appears to be dictated by interactions of PA26 Glu102 with the αPro17 reverse turn, especially with the main chain amide NH of αAsp18, and causes an expansion of the pore region diameter by about 1.6 Å (Table 1), which corresponds to an ~5 Å increase in circumference. Because the cluster residues αTyr8 and αAsp9 make intimate contacts with each other around the circumference of the gate, the expanded pore diameter appears necessary to accommodate the seven Tyr8/Asp9 residues in the ordered open conformation. In support of this proposal, we note that an isolated *A. fulgidus* proteasome α ring that adopts the open conformation also has its αPro17 residues at a diameter that is 1.6 Å larger than in the closed/disordered *A. fulgidus* proteasome structure (Groll et al., 2003) (Table 1).

Mechanism of Binding

Apart from the activation loop, the only contact between proteasome and PA26 is mediated by the C-terminal residues of PA26, which are known to provide major contributions to binding affinity of 11S activators (Li et al., 2000; Ma et al., 1993; Song et al., 1997). Details of this interaction were obscure in the low resolution yeast proteasome-PA26 complex (Förster et al., 2003; Whitby et al., 2000). The *T. acidophilum* proteasome-PA26 structures now reveal that the last three residues of PA26 (residues 229–231) contact the proteasome and are well ordered (Figure 5A), and that the other four residues following helix 4 (residues 225–228) serve as extended but relatively flexible tethers, as indicated by higher B factors, poorer density, and lack of stabilizing interactions.

The C-terminal three residues of PA26 make antiparallel β sheet-like hydrogen bonds with residues 78–82 of the proteasome α subunits. The only side chain that participates in significant interactions at this interface is proteasome αLys66, which hydrogen bonds with the PA26 C-terminal carboxylate. The use of main chain groups explains why 11S activators accommodate substantial variability in their C-terminal residues whereas deletion of just one residue abolishes PA28 activity (Li et al., 2000; Ma et al., 1993; Song et al., 1997). The importance of αLys66 for binding was confirmed by demonstrating that αLys66Ala and αLys66Ser proteasome, both of which are correctly assembled as indicated by gel filtration and wild-type levels of activity against small fluorogenic peptides, do not bind PA26 in a velocity sedimentation assay (Figure 5B) and do not further stimulate proteasomal peptidase activity (Figure 5C).

Difference maps of the rebuilt yeast proteasome-PA26 structure display density for four of the seven PA26 C termini that are consistent with the *T. acidophilum* proteasome-PA26 complex structures. All of the hydrogen bonds appear conserved in the occupied pockets, including between the PA26 C-terminal carboxylate and the αLys66 side chain. αLys66 is conserved in six of the seven pockets. The α7–α1 pocket has a tyrosine at this position, and not surprisingly, this pocket does not contain density for the PA26 C-terminal residues. The α6–α7 and α1–α2 pockets also lack density for the PA26 C-terminal residues, suggesting that for these pockets this region of PA26 is disordered and does not make stabilizing interactions. Because the α6–α7 and α1–α2 pockets each have a Lys66 residue appropriately located and simple docking on a graphics device does not reveal obvious steric impedi-

Table 1. Pore Diameters in Different Proteasome Structures

Proteasome[a]	PDB Code	Diameter (Å)[b]	State of Pore[c]
Yeast	1ryp (Groll et al., 1997)	37.2	closed
Bovine	1iru (Unno et al., 2002)	37.4	closed
Yeast α3ΔN	1g0u (Groll et al., 2000)	37.4	disordered
Yeast-PA26	This paper	40.3	open
T. acidophilum wild-type	1pma (Löwe et al., 1995)	38.5	disordered
T. acidophilum D9S-PA26	This paper	39.1	disordered
T. acidophilum Y8G/D9G-PA26	This paper	39.1	disordered
T. acidophilum wild-type-PA26	This paper	40.1	open
A. fulgidus	1j2p (Groll et al., 2003)	37.6	disordered
A. fulgidus α ring		39.3	open

[a] The structures of eukaryotic, *Thermoplasma acidophilum*, and *Archaeoglobus fulgidus* proteasomes are grouped separately and sorted from smallest to largest pore diameter.
[b] Diameters are defined as the average distance between αPro17 Cα atoms across the ring (i.e. the average of (α1–α3) + (α1–α4) + (α2–α4) + ..., etc.).
[c] The three possible states are closed and ordered, disordered before residue 13 (i.e. permeable to peptides but not to proteins), and open and ordered.

ments to binding, it is not clear why these two pockets are unoccupied. Presumably there are relatively subtle differences that favor/disfavor binding in the six pockets that contain αLys66. This is easy to envision, since the seven pockets of eukaryotic proteasomes are quite variable in their size, electrostatic potential, and identity of residues. For example, the α6–α7 pocket is relatively spacious, and a tyrosine that protrudes into the α1–α2 pocket might disfavor the αLys66-activator interaction. One possibility is that the different 11S activators, which have dissimilar C-terminal sequences, might bind into different subsets of the six pockets that house an αLys66.

Implications for Proteasome-PAN/PA700 Interactions

Bacteria contain a number of protease-activator complexes that are analogous to the proteasome (Gottesman, 2003). One of the best-studied examples is HslV-HslU, a hexameric double ring of HslV protease subunits bound to apical hexameric rings of HslU activator subunits (Missiakas et al., 1996). HslV shares the same overall fold and catalytic mechanism as the proteasome β subunits (Bochtler et al., 1997), and HslU, like PAN and PA700, belongs to the AAA+ ATPase superfamily (Neuwald et al., 1999; Zwickl et al., 1999). Remarkably, the PA26 C-terminal carboxylate-αLys66 interaction seen in our crystal structures is reminiscent of HslV-HslU; HslU C-terminal residues extend into a cleft between adjacent HslV subunits and the HslU C-terminal carboxylate hydrogen bonds with the side chain of a HslV lysine residue (Sousa et al., 2000; Wang et al., 2001). Although there are substantial differences in overall orientation that result from the equivalence of HslV with the proteasome β subunits rather than with α subunits, the contacts involve groups in HslV that are analogous to proteasome groups that contact PA26.

The unexpected similarity in binding for HslV-HslU and proteasome-PA26 prompted us to hypothesize that PA700 and PAN might also utilize an equivalent interaction. We tested this idea by subjecting αLys66Ala and αLys66Ser proteasome, neither of which bind PA26 (above), to a PAN-dependent proteolysis assay (Förster et al., 2003). Unlike wild-type *T. acidophilum* proteasome, which efficiently degrades casein in the presence of PAN and ATP, neither of these mutant proteasomes is able to degrade the protein substrate under the same conditions (Figure 6A). Because the structure suggests that these mutations are unlikely to destabilize the open gate conformation and, as noted earlier, these mutant proteasomes are assembled and active against peptide substrates, we conclude that the αLys66Ala/Ser mutant proteasomes are inactive in the proteolysis assay because they are unable to interact productively with PAN. To test this idea further, we constructed a PAN mutant in which the C-terminal residue was deleted and found that this truncated PAN was also deficient in the casein degradation assay (Figure 6B). The importance of αLys66 for proteasome function is consistent with its being invariant in an alignment of 18 available archaeal sequences (data not shown). Together, these observations support the model that PAN binds proteasome through a C-terminal carboxylate-αLys66 interaction that is equivalent to those of PA26.

Because PAN resembles the ATPases of PA700 (Zwickl et al., 1999), we propose that proteasome-PA700 interactions also mimic those of PA26. This suggestion has to address the expectation that PA700 is unlikely to share the 7-fold symmetry of PA26. Indeed, the most attractive model is that PA700 contacts proteasome through a pseudohexameric ring formed by its six different ATPase subunits (Köhler et al., 2001). Analogy with other AAA+ ATPases suggests that PAN also functions as a hexamer, although other arrangements are possible (Lee et al., 2003) and biophysical studies of PANs oligomeric state and binding to proteasome have been hampered by its poor behavior at accessible temperatures. (The host organism, *Methanococcus jannaschii*, shows optimal growth at 85°C, and PAN is inactive as an ATPase at 37°C or below [Zwickl et al., 1999]).

The likely mismatch of six PAN/PA700 subunits onto seven proteasome subunits can be understood from the available structural and sequence data. As discussed above, only six of the yeast proteasome subunits have a αLys66 residue, with the seventh subunit (α1) having a tyrosine at this position. Notably, an align-

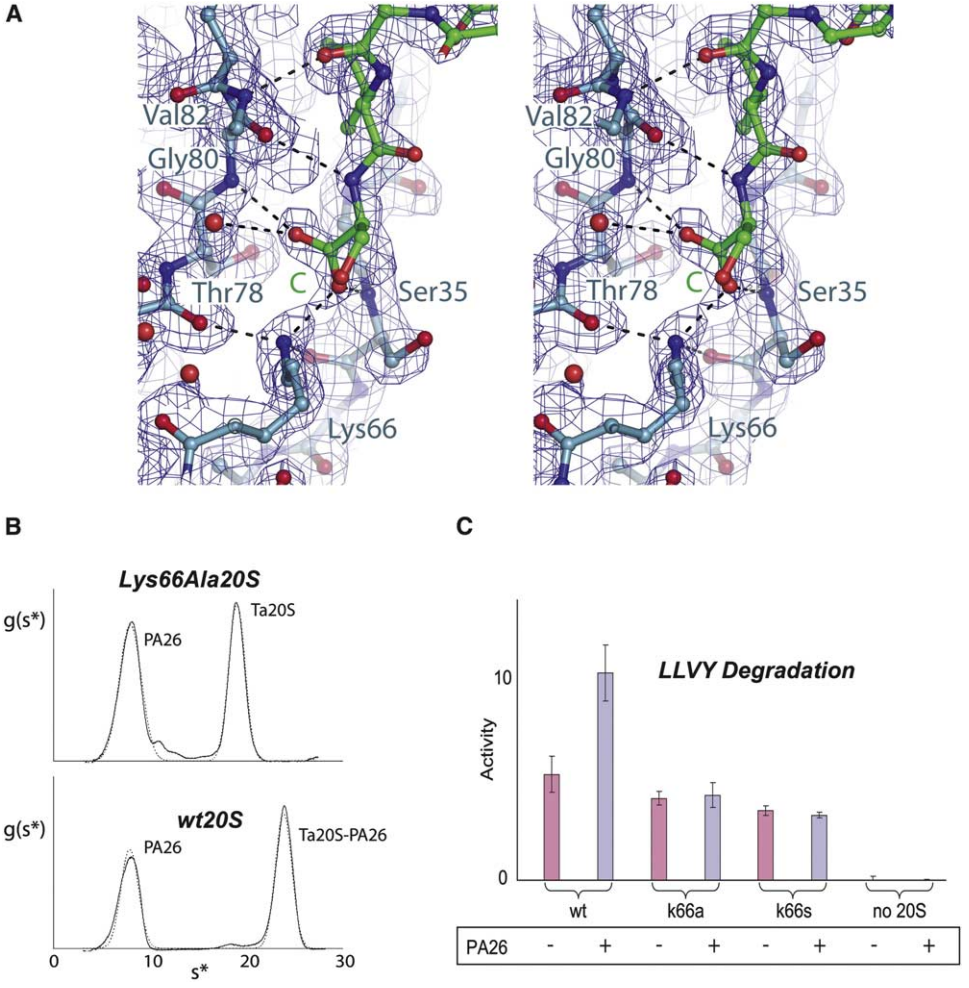

Figure 5. PA26-Proteasome Interaction

(A) Stereoview omit map of the PA26 C-terminal residues. Generated with PA26 residues 220–231 set to zero occupancy. Contoured at 1.0 × rmsd.

(B) Lys66Ala *T. acidophilum* proteasome fails to bind PA26 in a sedimentation velocity analytical ultracentrifugation assay. Top panel shows that a mixture of PA26 and Lys66Ala proteasome (molar ratio of 8:1) runs with same S* values as the separate components. Lys66Ser proteasome gives equivalent data. Bottom panel shows that PA26 forms a complex with wild-type proteasome that runs with a higher sedimentation coefficient. Raw data shown as solid lines, best fits as dotted lines.

(C) Lys66Ala and Lys66Ser *T. acidophilum* proteasome are not stimulated by PA26. The reaction mix (80 μl) contained 11.5 pmol proteasome (20S) and 92 pmol PA26 in buffer A (50 mM Tris [pH 7.5], 30 mM KCl, and 5 mM $MgCl_2$) at 37°C. The reaction was started by injecting 20 μl of an 80 μM solution of the small fluorogenic peptide substrate N-succinyl-Leu-Leu-Val-Tyr-7-amido-4-methylcoumarin. Activity (arbitrary units) was monitored by increase in fluorescence at 440 nm upon excitation at 380 nm in a BMG POLARstar Optima fluorimeter (BMG Labtechnologies, Durham, North Carolina). The error bars indicate standard deviations estimated from three experiments.

ment of eukaryotic proteasome sequences (Figure 6C) reveals that αLys66 is invariant in four of the pockets, while subunits α2 and α7 have either a lysine or are conservatively substituted by arginine. We note that the α2 and α7 pockets do not house ordered PA26 C termini in the yeast proteasome complex, although the significance of this correlation is unclear. The remaining subunit, α1, never has a lysine or arginine at this position. Thus, eukaryotic proteasome has just six pockets that are likely to be competent to bind the C-terminal tails of the six ATPase subunits of PA700.

The apparent mismatch of six hexameric C-terminal tails into six heptamerically arranged pockets might be accommodated by a flexible linker at the ATPase C termini. This would have parallels with the flexible linking residues observed in PA26 and HslU that connect their C-terminal proteasome/HslV binding residues to the body of the activator. Binding by C-terminal residues is in contrast to members of the bacterial ClpX/ClpA family of AAA^+ ATPase activators that mediate substrate delivery to the ClpP protease. ClpX and ClpA are hexamers that bind the heptameric ClpP through a 6:7 mismatched interface (Beuron et al., 1998). This interaction involves an internal loop of these activators (Guo et al., 2002; Kim and Kim, 2003; Kim et al., 2001; Singh et al., 2001), rather than their C termini, but as with our proposal for PAN and PA700, the mismatch appears to be accommodated by flexibility of residues connecting the

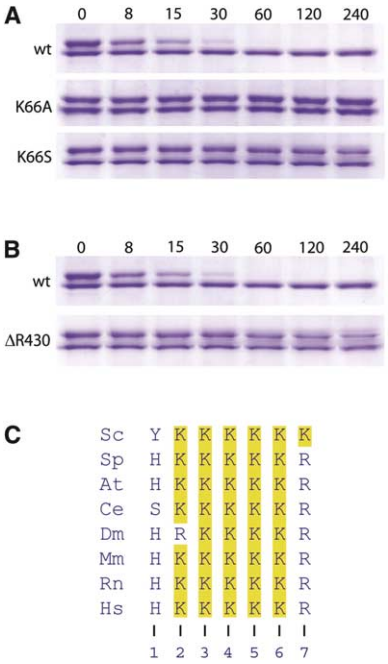

Figure 6. Binding of ATP-Dependent Activators

(A) PAN-dependent proteolysis requires proteasome αLys66. SDS-PAGE visualization of casein degradation assays with wild-type PAN, and wild-type, Lys66Ala, and Lys66Ser proteasomes as indicated. Top band is casein. Bottom band is proteasome, which serves as a loading control. Time in minutes is indicated above.

(B) PAN-dependent proteolysis requires C-terminal residue of PAN. Casein degradation assay with wild-type *T. acidophilum* proteasome and wild-type PAN or PAN truncated by one residue at the C terminus (ΔR430).

(C) Conservation of eukaryotic proteasome αLys66. The equivalent residue is shown for all seven subunits from eight eukaryotes. Sc, *Saccharomyces cerevisiae*; Sp, *Schizosaccharomyces pombe*; At, *Arabidopsis thaliana*; Ce, *Caenorhabditis elegans*; Dm, *Drosophila melanogaster*; Mm, *Mus musculus*; Rn, *Rattus norvegicus*; Hs, *Homo sapiens*.

protease binding residues to the body of the activator. Although we propose that binding by PAN and PA700 has analogy with that of PA26 and other 11S activators, the PA200 family of activators (Kajava et al., 2004; Ustrell et al., 2002), which are approximately the same size as an 11S heptamer but are monomeric and therefore lack an array of C termini for binding, must utilize an alternative mechanism.

In summary, the structures reported here explain how 11S activators bind proteasome despite their highly variable C-terminal sequences. The role of αLys66 and supporting biochemical studies indicate that although 11S activators function in part by imposing their 7-fold symmetry upon the proteasome gate, only six of the potential binding pockets of eukaryotic proteasome appear competent to bind 11S C termini and, as illustrated by the yeast proteasome-PA26 structure, the number of pockets occupied can be as few as four. The structures also indicate that formation of the ordered open conformation requires the four conserved residues αTyr8, αAsp9, αPro17, and αTyr26, and implies that the ability to form this conformation requires outward displacement of the αPro17 reverse turns to provide room for formation of the αTyr8-αAsp9 ring. We had previously noted that the ATP-dependent PAN and PA700 activators probably induce the same proteasome open conformation as stabilized by PA26 (Förster et al., 2003). The current work extends this parallel to imply that the ATP-dependent activators also employ a closely related mechanism of binding by inserting inherently flexible C-terminal residues into pockets where they form hydrogen bonding interactions with main-chain groups and the αLys66 side chain.

Experimental Procedures

Protein Purification and Activation Assays

Proteasome mutants were cloned and protein purified as described (Förster et al., 2003). PA26 was expressed and purified as described (Whitby et al., 2000; Yao et al., 1999). PAN mutants were generated using Stratagene's QuikChange protocol, except that RbCl-competent DH-5α cells were used for transformation in place of XL1-Blue supercompetent cells, and were purified as described (Zwickl et al., 1999). Casein degradation assays were performed as described (Förster et al., 2003).

Analytical Ultracentrifugation

Sedimentation velocity data were collected on a Beckman Optima XL-I analytical ultracentrifuge. Mixtures of proteasome and PA26 (1:1 to 1:8 molar ratio; final total protein concentration 0.9 mg/ml) in 20 mM Tris (pH 7.5), 200 mM NaCl, 2 mM DTT were centrifuged at 20°C at a rotor speed of 42,000 rpm. Immediately prior to centrifugation, protein was dialyzed into assay buffer and the used dialysis buffer retained as a blank for background correction. Two hundred interference measurements were recorded at 30 s intervals. Interference data were averaged and corrected for background against the blank. The program dcdt+ (Philo, 2000) was used for g(s*) analysis to determine the sedimentation coefficients.

Crystallization and Data Collection

PA26 and *T. acidophilum* proteasome were mixed at a molar ratio of 2.5:1 and concentrated to 10 mg/ml. Crystals of all three complexes were grown at 21°C using the hanging drop vapor diffusion method. The initial condition (0.1 M Na citrate/phosphate (pH 4.2), 0.2 M Li_2SO_4, 15% PEG 1000) was established for wild-type *T. acidophilum* proteasome-PA26 after initial screening using a Hydra 96+1 crystallization robot (Robbins Scientific, Sunnyvale, California) and sitting drop 96-well plates. In a local sparse matrix approach (Majeed et al., 2003), 10% of Crystal Screen 2 (Hampton Research, Aliso Viejo, California) was used to grid around the original condition. Addition of 1 M imidazole (pH 7.0) gave larger, more regular crystals. These were further improved by "feeding" (Bergfors, 2003), in which 2 μl of fresh protein solution was added to drops that contained a spray of tiny crystals.

Data were collected from two crystals of the wild-type complex and from single crystals of each mutant complex. Crystals were suspended in a nylon loop, rapidly cooled by plunging into liquid nitrogen, and maintained at 100 K for data collection. Prior to cooling, crystals were soaked in 0.1 M Na citrate/phosphate (pH 5.7), 0.2 M Li_2SO_4, 20% PEG 1000, and 30% glycerol. Data were collected at the National Synchrotron Light Source. The crystals belong to space group C2 and have half a complex in the asymmetric unit. The solvent content is 63%. Data were integrated and scaled with the HKL package (Otwinowski and Minor, 1997). See Supplemental Data for statistics.

Structure Determination and Refinement

Phases were obtained by molecular replacement using AMoRe (Navaza, 2001), with half a complex of wild-type *T. acidophilum* proteasome (pdb code 1pma) as the search model (Löwe et al., 1995). PA26 from the structure of the yeast proteasome-PA26 complex (Förster et al., 2003) was docked into residual density. Model building used the program O (Jones et al., 1991). Structure refine-

ment was initiated in CNS (Brünger et al., 1998) and completed in REFMAC5 (Murshudov, 1997), as provided in the CCP4 suite (Collaborative Computational Project, 1994). NCS constraints were not applied during refinement calculations. ARP/warp (Morris et al., 2003) was used in the modeling of some water molecules. Figures and structural alignments were created with PyMOL (DeLano, 2002).

Supplemental Data

Supplemental Data include a table and can be found with this article online at http://www.molecule.org/cgi/content/full/18/5/589/DC1/.

Acknowledgments

We thank Eric Ross for assistance with computer hardware and software, Lisa Joss for assistance with analytical ultracentrifugation, and Marty Rechsteiner and Wes Sundquist for critical comments on the manuscript. Operations of the National Synchrotron Light Source (NSLS) are supported by the U.S. Department of Energy, Office of Basic Energy Sciences, and by the National Institutes of Health. Data collection at the NSLS was funded by the National Center for Research Resources. This work was supported by National Institutes of Health (NIH) grant RO1 GM59135.

Received: January 4, 2005
Revised: April 18, 2005
Accepted: April 26, 2005
Published: May 26, 2005

References

Benaroudj, N., and Goldberg, A.L. (2000). PAN, the proteasome-activating nucleotidase from archaebacteria, is a protein-unfolding molecular chaperone. Nat. Cell Biol. *1*, 833–839.

Benaroudj, N., Zwickl, P., Seemüller, E., Baumeister, W., and Goldberg, A.L. (2003). ATP hydrolysis by the proteasome regulatory complex PAN serves multiple functions in protein degradation. Mol. Cell *11*, 69–78.

Bergfors, T. (2003). Seeds to crystals. J. Struct. Biol. *142*, 66–76.

Beuron, F., Maurizi, M.R., Belnap, D.M., Kocsis, E., Booy, F.P., Kessel, M., and Steven, A.C. (1998). At sixes and sevens: characterization of the symmetry mismatch of the ClpAP chaperone-assisted protease. J. Struct. Biol. *123*, 248–259.

Bochtler, M., Ditzel, L., Groll, M., Hartmann, C., and Huber, R. (1999). The proteasome. Annu. Rev. Biophys. Biomol. Struct. *28*, 295–317.

Bochtler, M., Ditzel, L., Groll, M., and Huber, R. (1997). Crystal structure of heat shock locus V (HslV) from Escherichia coli. Proc. Natl. Acad. Sci. USA *94*, 6070–6074.

Brünger, A.T., Adams, P.D., Clore, G.M., DeLano, W.L., Gros, P., Grosse-Kunstleve, R.W., Jiang, J.S., Kuszewski, J., Nilges, M., Pannu, N.S., et al. (1998). Crystallography & NMR system: A new software suite for macromolecular structure determination. Acta Crystallogr. D Biol. Crystallogr. *54*, 905–921.

Collaborative Computational Project, N. (1994). The CCP4 suite: programs for protein crystallography. Acta Crystallogr. D Biol. Crystallogr. *50*, 760–763.

DeLano, W.L. (2002). The CCP4 suite: programs for protein crystallography.

Dubiel, W., Pratt, G., Ferrell, K., and Rechsteiner, M. (1992). Purification of an 11 S regulator of the multicatalytic protease. J. Biol. Chem. *267*, 22369–22377.

Eleuteri, A.M., Kohanski, R.A., Cardozo, C., and Orlowski, M. (1997). Bovine spleen multicatalytic proteinase complex (proteasome). Replacement of X, Y, and Z subunits by LMP7, LMP2, and MECL1 and changes in properties and specificity. J. Biol. Chem. *272*, 11824–11831.

Förster, A., Whitby, F.G., and Hill, C.P. (2003). The pore of activated 20S proteasomes has an ordered 7-fold symmetric conformation. EMBO J. *22*, 4356–4364.

Gottesman, S. (2003). Proteolysis in bacterial regulatory circuits. Annu. Rev. Cell Dev. Biol. *19*, 565–587.

Groll, M., Bajorek, M., Köhler, A., Moroder, L., Rubin, D.M., Huber, R., Glickman, M.H., and Finley, D. (2000). A gated channel into the proteasome core particle. Nat. Struct. Biol. *7*, 1062–1067.

Groll, M., Brandstetter, H., Bartunik, H., Bourenkow, G., and Huber, R. (2003). Investigations on the maturation and regulation of archaebacterial proteasomes. J. Mol. Biol. *327*, 75–83.

Groll, M., Ditzel, L., Löwe, J., Stock, D., Bochtler, M., Bartunik, H.D., and Huber, R. (1997). Structure of 20S proteasome from yeast at 2.4Å resolution. Nature *386*, 463–471.

Guo, F., Maurizi, M.R., Esser, L., and Xia, D. (2002). Crystal structure of ClpA, an Hsp100 chaperone and regulator of ClpAP protease. J. Biol. Chem. *277*, 46743–46752.

Heinemeyer, W., Trondle, N., Albrecht, G., and Wolf, D.H. (1994). PRE5 and PRE6, the last missing genes encoding 20S proteasome subunits from yeast? Indication for a set of 14 different subunits in the eukaryotic proteasome core. Biochemistry *33*, 12229–12237.

Hilt, W., Heinemeyer, W., and Wolf, D.H. (1993). Studies on the yeast proteasome uncover its basic structural features and multiple in vivo functions. Enzyme Protein *47*, 189–201.

Jones, T.A., Zou, J.Y., Cowan, S.W., and Kjeldgaard, M. (1991). Improved methods for building protein models in electron density maps and the location of errors in these models. Acta Crystallogr. A *47*, 110–119.

Kajava, A.V., Gorbea, C., Ortega, J., Rechsteiner, M., and Steven, A.C. (2004). New HEAT-like repeat motifs in proteins regulating proteasome structure and function. J. Struct. Biol. *146*, 425–430.

Kim, D.Y., and Kim, K.K. (2003). Crystal structure of ClpX molecular chaperone from Helicobacter pylori. J. Biol. Chem. *278*, 50664–50670.

Kim, Y.I., Levchenko, I., Fraczkowska, K., Woodruff, R.V., Sauer, R.T., and Baker, T.A. (2001). Molecular determinants of complex formation between Clp/Hsp100 ATPases and the ClpP peptidase. Nat. Struct. Biol. *8*, 230–233.

Knowlton, J.R., Johnston, S.C., Whitby, F.G., Realini, C., Zhang, Z., Rechsteiner, M., and Hill, C.P. (1997). Structure of the proteasome activator REGalpha (PA28alpha). Nature *390*, 639–643.

Köhler, A., Cascio, P., Leggett, D.S., Woo, K.M., Goldberg, A.L., and Finley, D. (2001). The axial channel of the proteasome core particle is gated by the Rpt2 ATPase and controls both substrate entry and product release. Mol. Cell *7*, 1143–1152.

Kopp, F., Hendil, K.B., Dahlmann, B., Kristensen, P., Sobek, A., and Uerkvitz, W. (1997). Subunit arrangement in the human 20S proteasome. Proc. Natl. Acad. Sci. USA *94*, 2939–2944.

Lee, S.Y., De La Torre, A., Yan, D., Kustu, S., Nixon, B.T., and Wemmer, D.E. (2003). Regulation of the transcriptional activator NtrC1: structural studies of the regulatory and AAA+ ATPase domains. Genes Dev. *17*, 2552–2563.

Li, J., Gao, X., Joss, L., and Rechsteiner, M. (2000). The proteasome activator 11 S REG or PA28: chimeras implicate carboxyl-terminal sequences in oligomerization and proteasome binding but not in the activation of specific proteasome catalytic subunits. J. Mol. Biol. *299*, 641–654.

Löwe, J., Stock, D., Jap, B., Zwickl, P., Baumeister, W., and Huber, R. (1995). Crystal structure of the 20S proteasome from the archaeon T. acidophilum at 3.4 A resolution. Science *268*, 533–539.

Ma, C.P., Slaughter, C.A., and DeMartino, G.N. (1992). Identification, purification, and characterization of a protein activator (PA28) of the 20 S proteasome (macropain). J. Biol. Chem. *267*, 10515–10523.

Ma, C.P., Willy, P.J., Slaughter, C.A., and DeMartino, G.N. (1993). PA28, an activator of the 20 S proteasome, is inactivated by proteolytic modification at its carboxyl terminus. J. Biol. Chem. *268*, 22514–22519.

Majeed, S., Ofek, G., Belachew, A., Huang, C.C., Zhou, T., and Kwong, P.D. (2003). Enhancing protein crystallization through precipitant synergy. Structure *11*, 1061–1070.

Missiakas, D., Schwager, F., Betton, J.M., Georgopoulos, C., and Raina, S. (1996). Identification and characterization of HslV HslU (ClpQ ClpY) proteins involved in overall proteolysis of misfolded proteins in Escherichia coli. EMBO J. *15*, 6899–6909.

Morris, R.J., Perrakis, A., and Lamzin, V.S. (2003). ARP/wARP and automatic interpretation of protein electron density maps. Methods Enzymol. *374*, 229–244.

Murshudov, G.N. (1997). Refinement of macromolecular structures by the maximum-likelihood method. Acta Crystallogr. D Biol. Crystallogr. *53*, 240–255.

Mykles, D.L. (1996). Differential effects of bovine PA28 on six peptidase activities of the lobster muscle proteasome (multicatalytic proteinase). Arch. Biochem. Biophys. *325*, 77–81.

Navaza, J. (2001). Implementation of molecular replacement in AMoRe. Acta Crystallogr. D Biol. Crystallogr. *57*, 1367–1372.

Neuwald, A.F., Aravind, L., Spouge, J.L., and Koonin, E.V. (1999). AAA+: A class of chaperone-like ATPases associated with the assembly, operation, and disassembly of protein complexes. Genome Res. *9*, 27–43.

Otwinowski, Z., and Minor, W. (1997). Processing of X-ray diffraction data collected in oscillation mode. Methods Enzymol. *276*, 307–326.

Philo, J.S. (2000). A method for directly fitting the time derivative of sedimentation velocity data and an alternative algorithm for calculating sedimentation coefficient distribution functions. Anal. Biochem. *279*, 151–163.

Rechsteiner, M., and Hill, C.P. (2005). Mobilizing the proteolytic machine: cell biological roles of proteasome activators and inhibitors. Trends Cell Biol. *15*, 27–33.

Singh, S.K., Rozycki, J., Ortega, J., Ishikawa, T., Lo, J., Steven, A.C., and Maurizi, M.R. (2001). Functional domains of the ClpA and ClpX molecular chaperones identified by limited proteolysis and deletion analysis. J. Biol. Chem. *276*, 29420–29429.

Song, X., von Kampen, J., Slaughter, C.A., and DeMartino, G.N. (1997). Relative functions of the α and β subunits of the proteasome activator, PA28. J. Biol. Chem. *272*, 27994–28000.

Sousa, M.C., Trame, C.B., Tsuruta, H., Wilbanks, S.M., Reddy, V.S., and McKay, D.B. (2000). Crystal and solution structures of an HslUV protease-chaperone complex. Cell *103*, 633–643.

Unno, M., Mizushima, T., Morimoto, Y., Tomisugi, Y., Tanaka, K., Yasuoka, N., and Tsukihara, T. (2002). The structure of the mammalian 20S proteasome at 2.75 Å resolution. Structure *10*, 609–618.

Ustrell, V., Hoffman, L., Pratt, G., and Rechsteiner, M. (2002). PA200, a nuclear proteasome activator involved in DNA repair. EMBO J. *21*, 3516–3525.

Velichutina, I., Connerly, P.L., Arendt, C.S., Li, X., and Hochstrasser, M. (2004). Plasticity in eucaryotic 20S proteasome ring assembly revealed by a subunit deletion in yeast. EMBO J. *23*, 500–510.

Wang, J., Song, J.J., Franklin, M.C., Kamtekar, S., Im, Y.J., Rho, S.H., Seong, I.S., Lee, C.S., Chung, C.H., and Eom, S.H. (2001). Crystal structures of the HslVU peptidase-ATPase complex reveal an ATP-dependent proteolysis mechanism. Structure *9*, 177–184.

Whitby, F.G., Masters, E.I., Kramer, L., Knowlton, J.R., Yao, Y., Wang, C.C., and Hill, C.P. (2000). Structural basis for the activation of 20S proteasomes by 11S regulators. Nature *408*, 115–120.

Yao, Y., Huang, L., Krutchinsky, A., Wong, M.L., Standing, K.G., Burlingame, A.L., and Wang, C.C. (1999). Structural and functional characterization of the proteasome-activating protein PA26 from Trypanosoma brucei. J. Biol. Chem. *274*, 33921–33930.

Zhang, Z., Clawson, A., Realini, C., Jensen, C.C., Knowlton, J.R., Hill, C.P., and Rechsteiner, M. (1998). Identification of an activation region in the proteasome activator REGalpha. Proc. Natl. Acad. Sci. USA *95*, 2807–2811.

Zwickl, P., Ng, D., Woo, K.M., Klenk, H.P., and Goldberg, A.L. (1999). An archaebacterial ATPase, homologous to ATPases in the eukaryotic 26 S proteasome, activates protein breakdown by 20 S proteasomes. J. Biol. Chem. *274*, 26008–26014.

Accession Numbers

Protein Data Bank entry codes are: 1ya7, wild-type *T. acidophilum* proteasome-PA26; 1yar, D9S-PA26; 1yau, GG-PA26; 1z7q, yeast proteasome-PA26.

Supplemental Data

The 1.9 Å Structure of a Proteasome-11S Activator Complex and Implications for Proteasome-PAN/PA700 Interactions

Andreas Förster, Eugene I. Masters, Frank G. Whitby, Howard Robinson, and Christopher P. Hill

Supplemental Table

Table S1. Crystallographic Statistics

Data Set[a]	Ta20S–PA26	Ta20Sgg–PA26	Ta20Sd9s–PA26
Space group a, b, c (Å) β (°)	C2 255.7, 127.0, 181.5 92.6	C2 255.2, 126.9, 181.0 92.4	C2 254.9, 127.5, 181.2 92.5
Data Collection[b]			
Resolution[c] (Å) Beamline Wavelength (Å) Total/unique observations R_{merge}[d] (%) Completeness (%) I/σ(I)	20-2.3 (2.38-2.30) X25 1.283 2,009,533 / 257,676 11.6 (67.5) 100.0 (100.0) 8.0 (2.2)	20-2.4 (2.49-2.40) X29 1.0722 909,044 / 224,164 8.7 (38.1) 99.9 (99.9) 9.0 (2.1)	20-1.9 (1.97-1.90) X25 1.283 2,194,276 / 442,007 6.3 (49.7) 97.4 (95.8) 10.0 (2.2)
Refinement Statistics			
Residues modeled: PA26 Ta20S α subunits Ta20S β subunits # mols: H_2O/glycerol/SO_4 R_{factor}[e] / R_{free}[f] (%) <B> values (A^2): 20Sα / 20Sβ / PA26 H_2O / glycerol / SO_4 ϕ/ψ most favored (%) Rmsd bond: Lengths (Å)/ angles (°)	 4-161, 172-231 7-233 1-203 1,659/ 7/ 21 18.0 / 22.4 46.8 / 40.3 / 47.7 48.4 / 48.9 / 68.7 92.3 0.015 / 1.464	 4-161, 172-231 12-233 1-203 1,571/ 7/ 21 18.0 / 23.3 42.8 / 33.0 / 45.4 41.5 / 43.7 / 75.1 92.0 0.017 / 1.585	 4-161, 172-231 13-233 1-203 3,470/ 7/ 21 18.2 / 21.6 33.5 / 27.2 / 30.2 42.5 / 36.5 / 60.0 94.0 0.012 / 1.271

[a]Ta20S = *Thermoplasma acidophilum* 20S proteasome. Ta20Sgg= Tyr8Gly, Asp9Gly mutant. Ta20Sd9s = Asp9Ser mutant.

[b]All data were collected at the National Synchrotron Light Source at Brookhaven National Laboratory.

[c]Values in parenthesis refer to the highest resolution shell.

[d]$R_{merge} = \Sigma_h\Sigma_i |I_i(h) <I(h)>|/\Sigma_h\Sigma_i I(h)$, where $I_i(h)$ is the ith measurement and $<I(h)>$ the mean of I(h)

[e]$R_{factor} = \Sigma_h||F_o(h)| - |F_c(h)|| / \Sigma_h|F_o(h)|$.

[f]R_{free} = R_{factor} calculated for 991 (wt), 1069 (GG) or 1345 (D9S) reflections from each complex that were not used in refinement calculations.